Measurement of the Entanglement between Photonic Spatial Modes in Optical Fibers

Yoonshik Kang,[1] Jaekwon Ko,[2] Sang Min Lee,[1] Sang-Kyung Choi,[1] Byoung Yoon Kim,[2] and Hee Su Park[1,*]

[1]*Korea Research Institute of Standards and Science, Daejeon 305-340, South Korea*

[2]*Department of Physics, Korea Advanced Institute of Science and Technology, Daejeon 305-701, South Korea*

(Received 27 March 2012; revised manuscript received 11 June 2012; published 10 July 2012)

We experimentally demonstrate the entanglement of spatial modes between two photons propagating through separate few-mode optical fibers. Quantum states over the two lowest-order spatial modes are measured with highly efficient spatial-mode analyzers based on acousto-optics. Quantum state tomography verifies the entanglement of the spatial-domain Bell state.

DOI: 10.1103/PhysRevLett.109.020502 PACS numbers: 03.67.Bg, 03.67.Hk, 42.50.Dv, 42.81.Wg

Photonic entanglement in various degrees of freedom is a key resource of quantum communication protocols. Polarization [1–5], path [6], time-bin [7], color [8], and orbital angular momentum (OAM) [9–12] have been used as quantum information carriers. The advantages of spatial modes, such as those denoted by OAM eigenstates, are the intrinsically infinite dimension and the possibility of realizing hyperentanglement or hybrid entanglement in combination with photonic polarization. Twelve-dimensional entanglement has been demonstrated with OAM eigenstates [13], and hyperentanglement of OAM and polarization has been used to demonstrate superdense coding, beating the classical channel capacity limit [14].

The comparative advantage of optical fibers over free space as channels for light propagation can be applied to the transmission of entangled photons [2,4,7,8,15]. Spatial entanglement can also be transmitted through optical fibers designed to guide multiple spatial modes. A recent work has demonstrated the transmission of spatial-mode-entangled single photons through a hollow-core fiber that can guide three spatial modes [16]. However, measurements of spatial mode entanglement over multiple fiber modes have been limited by technical difficulties to less than fully arbitrary superposition states. For example, the measurement with a step-phase plate for one photon of an entangled pair in [16] is only applicable to states in the form of $\sin\theta|0\rangle + \cos\theta|1\rangle$ with real θ.

In this work, we demonstrate the measurement of a larger set of spatial-mode-entangled two-photon states that propagate within two few-mode fibers. Each fiber contains an efficient photonic spatial-mode analyzer, which consists of an acousto-optic mode converter (AOMC) and a mode stripper. The measurement basis is electrically controlled by the amplitude and phase of the rf signal applied to the acousto-optic (AO) transducer. The all-fiber configuration of the spatial-mode analyzer is highly efficient with low insertion loss because photons stay within the fiber throughout the mode conversion and filtering process. The spatial-mode analyzers are aligned to compensate for a dephasing effect caused by the continuous phase change of the acoustic waves. The measurement scheme is extendable to states spanning more than two spatial modes by driving the AOMCs with multifrequency signals.

The optical fiber used in our experiments is a polarization-maintaining, step-index fiber (Thorlabs PM1300-HP) that can guide the three lowest-order spatial modes (LP_{01}, even LP_{11}, and odd LP_{11}) within the wavelength range of interest ($\sim$ 810 nm). Here, the LP_{11} modes are linearly polarized modes with antisymmetric field profiles. While a perfectly circular fiber has nonlinearly polarized, second-order spatial modes (e.g., HE_{21}, TM_{01}, and TE_{01}) with rotationally symmetric intensity profiles, the fiber in this work has a specific axis of symmetry due to stress-applying materials and therefore has LP_{11} modes as its eigenmodes. Even and odd modes refer to modes whose lobe orientations are parallel and perpendicular, respectively, to the axis of symmetry. The difference between the propagation constants of the two LP_{11} modes allows clear mode discrimination by acousto-optic interaction. The experiments in our work measure only one of the two LP_{11} modes, specifically, the "even" mode: All photons in the "odd" LP_{11} mode are removed by a mode stripper, as explained below. We, henceforth, let the term "LP_{11} mode" represent only the even mode and call the fiber "a two-mode fiber" (TMF) to avoid confusion.

The structure of the spatial-mode analyzer and the measured mode profiles are shown in Fig. 1. An rf electric signal drives a shear-mode piezoelectric transducer (PZT) to generate a flexural acoustic wave, which is focused by a glass horn onto an unjacketed fiber section. The acoustic wave creates periodic asymmetric perturbations of the optical path length within the fiber and couples the symmetric LP_{01} mode with the antisymmetric LP_{11} mode. Efficient coherent coupling between the two modes depends on matching the acoustic wavelength, tuned by the rf frequency, to the beat length $\Lambda = \lambda/(n_{LP_{01}} - n_{LP_{11}})$, where λ and n_i, respectively, are the photon wavelength and the effective refractive index of mode i [17]. The mode conversion efficiency is determined by the magnitude of the acoustically generated microbends and is controllable with the amplitude of the electric signal. A mode stripper is a fiber section that is wound one turn with a diameter of 6 mm. The more weakly guided LP_{11}

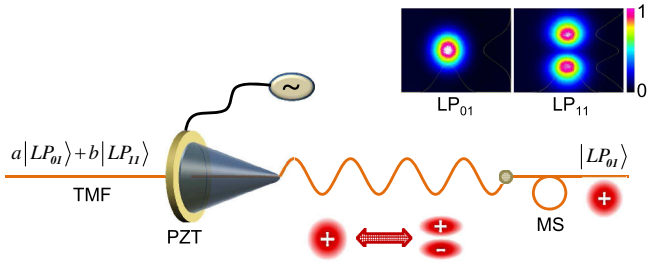

FIG. 1 (color online). Structure of the spatial-mode analyzer. Inset: intensity distributions of the LP_{01} and LP_{11} modes. An electrically driven shear-mode piezoelectric transducer (PZT) excites a flexural acoustic wave that is focused by a glass horn onto an unjacketed fiber section. Acoustically generated periodic microbends induce coherent coupling between the two spatial modes. A mode stripper (MS) removes only the LP_{11} mode from the fiber core through mode-dependent bending loss. TMF: two-mode fiber.

mode undergoes higher bending loss than the fundamental LP_{01} mode: >97% of the light in the LP_{11} mode radiates out, whereas the LP_{01} mode has insignificant loss. Therefore, the mode stripper projects an input state to an LP_{01} state with an extinction ratio of <3%. A side effect of the mode conversion process is the down-shift or up-shift of the optical frequency according to the mode configuration [18]. The photon in the final mode is frequency up-shifted (down-shifted) when its momentum, or wave vector, is generated by adding (subtracting) the acoustic momentum to (from) the photonic momentum in the initial mode. Here, the phase of the rf signal adds a phase factor to the photonic state in the converted mode.

A schematic of the experimental setup is shown in Fig. 2. Entangled photon pairs are generated by type-I spontaneous parametric down-conversion (SPDC) in a 1-mm-thick beta-barium borate (BBO) crystal pumped by a single transverse- and longitudinal-mode cw diode laser (wavelength 405 nm, output power 40 mW, $1/e^2$ diameter 0.36 mm). The polarization of the photons is horizontal after the SPDC crystal and linear along the axis of symmetry inside the TMF. Each photon is collimated by a lens (not shown in the figure; focal length 250 mm) and then coupled to a TMF through an aspheric lens (focal length 15.4 mm). This lens projects the symmetric LP_{01} mode and the antisymmetric LP_{11} mode of the TMF to conjugate images of symmetric and antisymmetric profiles ($1/e^2$ diameters of 0.15 mm), respectively, inside the crystal. The transverse field profile of the pump laser is ideally symmetric, then by parity conservation, the down-converted two-photon state $|\psi\rangle$ that couples to the TMFs becomes a coherent superposition of two direct-product

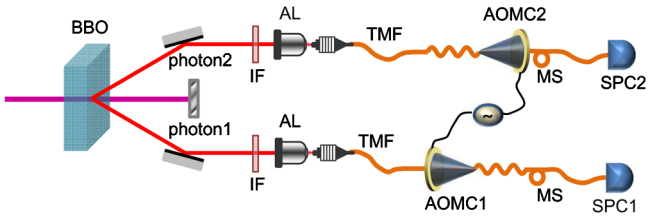

FIG. 2 (color online). Schematic of the experimental setup. Photon pairs are generated by type-I SPDC in a BBO crystal and coupled to two-mode fibers (TMFs) through aspheric lenses. AOMC: acousto-optic mode converter, MS: mode stripper, SPC: single-photon counter, AL: aspheric lens, IF: interference filter (half-maximum bandwidth of 2 nm).

states where both photons are symmetric (LP_{01}) or antisymmetric (LP_{11}):

$$|\psi\rangle = a|\mathrm{LP}_{01}\rangle|\mathrm{LP}_{01}\rangle + b|\mathrm{LP}_{11}\rangle|\mathrm{LP}_{11}\rangle. \quad (1)$$

Here, a and b are constants that depend on the pump beam spatial profile, the fiber geometry, and the imaging optics configuration. As shown by the analysis on the spiral bandwidth of OAM-entangled states [19], increasing the pump beam width (or reducing the crystal thickness) increases the second term in Eq. (1) to the level of the first-order term, resulting in a maximally entangled state. The ratio a/b in our experiments is set to achieve a compromise between entanglement quality and photon generation rate. After propagating through a 40-cm TMF section, each photon enters an AOMC and a mode stripper. Output photons from the mode strippers are measured with single-mode-fiber-coupled photon counters (Perkin Elmer SPCM-AQ4C) and NIM-based coincidence logic units. As each photon counter counts the photons in the LP_{01} mode, the LP_{01}- and the LP_{11}-mode basis states of the input to the AOMC are measured by completely turning the AOMC off and on, respectively, while superposition states are measured by setting a conversion efficiency between 0 and 1.

The two acoustic transducers are aligned such that the two acoustic waves propagate in mutually opposite directions along the respective fibers. This alignment eliminates from the entanglement measurement the effect of the phase shift induced by the traveling acoustic waves. When LP_{11}-mode photons are converted to LP_{01}-mode photons by an acoustic wave propagating in the same (opposite) direction as the photons, the optical frequency of the photons is up-shifted (down-shifted). Therefore, the two-photon state $|\psi_{\mathrm{meas}}\rangle$ measured with the transducers aligned oppositely as in Fig. 2 can be expressed as:

$$\begin{aligned}|\psi_{\mathrm{meas}}\rangle &= (\sqrt{1-\eta_1}|\mathrm{LP}_{01}\rangle + \sqrt{\eta_1}e^{i\Delta t+\phi_1}|\mathrm{LP}_{11}\rangle)\cdot(\sqrt{1-\eta_2}|\mathrm{LP}_{01}\rangle + \sqrt{\eta_2}e^{-i\Delta t+\phi_2}|\mathrm{LP}_{11}\rangle)\\ &= \sqrt{(1-\eta_1)(1-\eta_2)}|\mathrm{LP}_{01}\rangle|\mathrm{LP}_{01}\rangle + \sqrt{(1-\eta_1)\eta_2}e^{-i\Delta t+\phi_2}|\mathrm{LP}_{01}\rangle|\mathrm{LP}_{11}\rangle + \sqrt{\eta_1(1-\eta_2)}e^{i\Delta t+\phi_1}|\mathrm{LP}_{11}\rangle|\mathrm{LP}_{01}\rangle\\ &\quad + \sqrt{\eta_1\eta_2}e^{\phi_1+\phi_2}|\mathrm{LP}_{11}\rangle|\mathrm{LP}_{11}\rangle, \quad (2)\end{aligned}$$

where η_i is the conversion efficiency of AOMCi, Δ is the acoustic frequency, and ϕ_i is the phase of the driving signal for AOMCi. Since the acoustic time period $1/\Delta$ is much smaller than the unit coincidence counting duration (> 1 s), the acoustically induced frequency shift averages out the phase of the $|\mathrm{LP}_{01}\rangle|\mathrm{LP}_{11}\rangle$ and $|\mathrm{LP}_{11}\rangle|\mathrm{LP}_{01}\rangle$ components. This phase information can be retrieved if a time-resolved measurement is applied to the beating signals. In contrast, the relative phase between the terms associated with $|\mathrm{LP}_{01}\rangle|\mathrm{LP}_{01}\rangle$ and $|\mathrm{LP}_{11}\rangle|\mathrm{LP}_{11}\rangle$ is not affected by the acoustic frequency shift. This allows a Bell state in the form of Eq. (1) to be measured without being disturbed. When the input state includes terms involving $|\mathrm{LP}_{01}\rangle|\mathrm{LP}_{11}\rangle$ or $|\mathrm{LP}_{11}\rangle|\mathrm{LP}_{01}\rangle$ in addition to Eq. (1), the coherence due to these terms, i.e., the off-diagonal elements of the density matrix that includes these terms, is measured to be zero regardless of their real values.

The fabricated AOMC has an AO interaction length of 90 mm. This section of the TMF is unjacketed and etched such that the outer cladding diameter is 59 μm. The etching enhances the coupling efficiency by a factor of 6.5 compared to an AOMC with the original cladding diameter of 125 μm [20]. The acoustic frequency is 2.1 MHz, resulting in an acoustic wavelength of 470 μm. The AOMC is characterized as shown in Fig. 3(a) by a measurement of the transmission spectra using a broadband source, where the input is fixed as $|\mathrm{LP}_{01}\rangle$ by placing another mode stripper (not shown in Fig. 2) in front of the AOMC. Notches appearing in the transmission spectra indicate the conversion of the input LP_{01} mode to the LP_{11} mode via removal by a mode stripper. The center wavelength of AO conversion is tunable as 0.6 nm/kHz around 2.1 MHz. Figure 3(b) shows the conversion efficiency for a center wavelength of 810 nm as the driving voltage is varied, reaching a maximum of 92% at a voltage of 5.3 V_{pp} and decreasing at higher voltages due to overcoupling. This efficiency is measured by coincidence counts of photon pairs with the input state fixed as $|\mathrm{LP}_{01}\rangle|\mathrm{LP}_{01}\rangle$ and operating only one of the AOMCs shown in Fig. 2. Regarding the 8% deviation from the perfect mode conversion, 5% can be accounted for by the finite wavelength bandwidth of the AOMC as shown in Fig. 3(a): the efficiency becomes lower near the band edge. The remaining 3% is attributable to nonidealness in the AO interaction and the mode stripper, where the contribution of each factor is unclear. We expect that the conversion efficiency can be improved by an AOMC with a higher bandwidth using a fiber with two spatial modes having the same group velocity [21], and by optimization of acoustic impedance matching and mode stripper design.

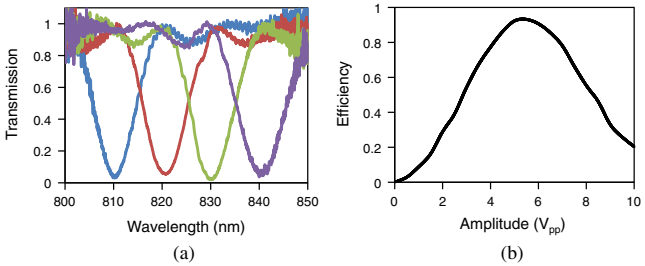

FIG. 3 (color online). Performance of the mode converter. (a) Transmission spectra for LP_{01}-mode input. Driving frequencies are 2.062 MHz (leftmost notch), 2.078 MHz, 2.094 MHz, and 2.110 MHz (rightmost notch). (b) Conversion efficiency at 810 nm when driven at 2.062 MHz.

We verify the spatial-mode correlation corresponding to each term in Eq. (1) by coincidence counting of photons projected to $|\mathrm{LP}_{01}\rangle$ or $|\mathrm{LP}_{11}\rangle$, as shown in Fig. 4(a). The coherence between the two terms in Eq. (1) is verified by measuring the coincidence fringes with each photon being projected to a superposition state $1/\sqrt{2}(|\mathrm{LP}_{01}\rangle + e^{i\phi}|\mathrm{LP}_{11}\rangle)$, where ϕ is a phase factor. The sinusoidal fringes with a visibility of 85%, as shown in Fig. 4(b), are clear evidence of the coherence between the two biphoton states of Eq. (1). Figure 5(a) shows a quantitative measurement of the entanglement by quantum state tomography (QST) with a set of 16 projections and maximum likelihood estimation [22]. The concurrence calculated from the resulting density matrix ρ in Fig. 5(b) is 0.70 ± 0.01, where the error denotes the statistical uncertainty $\pm\sqrt{\text{counts}}$. The purity of the reconstructed state, $\mathrm{Tr}\{\rho^2\}$, is 0.77 ± 0.01. The effect of imperfect mode conversion on QST can be approximately compensated for with the simple assumption that the $|\mathrm{LP}_{11}\rangle$ in Fig. 5(a) can be replaced by a coherent superposition of 8% of $|\mathrm{LP}_{01}\rangle$ and 92% of $|\mathrm{LP}_{11}\rangle$. The revised calculation yields higher values for concurrence and purity: 0.83 and 0.91, respectively. Since the original state $|\psi\rangle$ described by Eq. (1) is expected to have a concurrence of 0.94 due to the imbalance between the $|\mathrm{LP}_{01}\rangle|\mathrm{LP}_{01}\rangle$ and $|\mathrm{LP}_{11}\rangle|\mathrm{LP}_{11}\rangle$ components, we estimate that unwanted $|\mathrm{LP}_{01}\rangle|\mathrm{LP}_{11}\rangle$ and $|\mathrm{LP}_{11}\rangle|\mathrm{LP}_{01}\rangle$ components and other imperfections cause a 10% reduction in the concurrence.

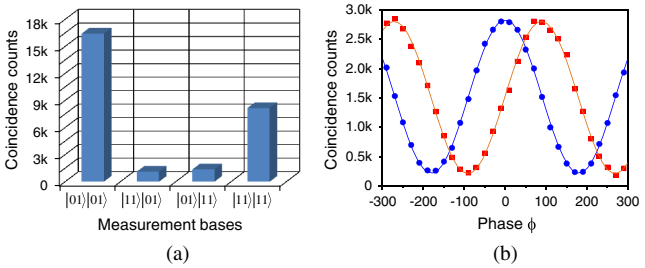

FIG. 4 (color online). Two-photon correlation measurements. (a) Coincidence counts for 50 s with each photon projected to either $|\mathrm{LP}_{01}\rangle$ or $|\mathrm{LP}_{11}\rangle$. (b) Coincidence counts for 10 s: Photon 1 is projected to $(|\mathrm{LP}_{01}\rangle + |\mathrm{LP}_{11}\rangle)/\sqrt{2}$ (circle) and $(|\mathrm{LP}_{01}\rangle + i|\mathrm{LP}_{11}\rangle)/\sqrt{2}$ (square). Photon 2 is projected to $(|\mathrm{LP}_{01}\rangle + e^{i\phi}|\mathrm{LP}_{11}\rangle)/\sqrt{2}$ with varying ϕ. The phase between $|\mathrm{LP}_{01}\rangle$ and $|\mathrm{LP}_{11}\rangle$ is the same as the phase of the rf signals applied to the two AOMCs.

(a)

photon 1	photon 2	counts	photon 1	photon 2	counts
$\|LP_{01}\rangle$	$\|LP_{01}\rangle$	16423	$\|D\rangle$	$\|LP_{01}\rangle$	8372
$\|LP_{01}\rangle$	$\|LP_{11}\rangle$	1127	$\|D\rangle$	$\|LP_{11}\rangle$	5515
$\|LP_{11}\rangle$	$\|LP_{01}\rangle$	1356	$\|D\rangle$	$\|D\rangle$	12055
$\|LP_{11}\rangle$	$\|LP_{11}\rangle$	8168	$\|D\rangle$	$\|R\rangle$	6408
$\|LP_{01}\rangle$	$\|D\rangle$	8438	$\|R\rangle$	$\|LP_{01}\rangle$	8517
$\|LP_{01}\rangle$	$\|R\rangle$	8340	$\|R\rangle$	$\|LP_{11}\rangle$	4721
$\|LP_{11}\rangle$	$\|D\rangle$	5512	$\|R\rangle$	$\|D\rangle$	6448
$\|LP_{11}\rangle$	$\|R\rangle$	5725	$\|R\rangle$	$\|R\rangle$	907

(b)

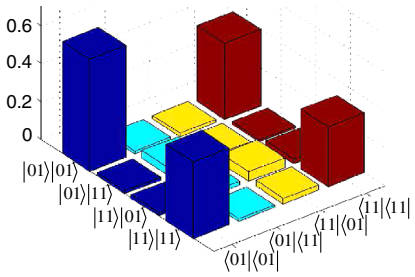

FIG. 5 (color online). Results of quantum state tomography. (a) Coincidence counts for 50 s. $|D\rangle = (|\mathrm{LP}_{01}\rangle + |\mathrm{LP}_{11}\rangle)/\sqrt{2}$, $|R\rangle = (|\mathrm{LP}_{01}\rangle - i|\mathrm{LP}_{11}\rangle)/\sqrt{2}$. (b) Absolute magnitude of the reconstructed density matrix elements. The imaginary part of every density matrix element is less than 0.033.

This measurement scheme can be extended to more than two modes. Our AOMC can convert the LP_{01} mode to an LP_{1i} mode, with $i > 1$, with a change in the acoustic frequency. Here, the LP_{1i} modes have the same symmetry as the LP_{11} mode but with a larger number of lobes along the radial direction. Multimode operation can be realized by driving the acoustic transducer with a linear superposition of multiple rf signals to generate an acoustic wave that, in turn, is also a linear superposition of rf components, which induces multiple mode couplings. The amplitude and phase of each component can be independently controlled. Such a multifrequency, multimode operation has been demonstrated in the context of an electronically controllable wavelength filter that couples the LP_{01} mode to multiple LP_{1i} cladding modes [23]. We believe that the reverse process, conversion from a superposition state to $|\mathrm{LP}_{01}\rangle$, is possible with the same device. General multimode entangled states measurable with the setup in Fig. 2 are of the form

$$|\psi\rangle = c_0|\mathrm{LP}_{01}\rangle|\mathrm{LP}_{01}\rangle + \sum_{i\geq 1} c_i|\mathrm{LP}_{1i}\rangle|\mathrm{LP}_{1i}\rangle, \qquad (3)$$

where the c_i values are complex constants. In contrast, the parallel alignment of the two AOMCs enables the detection of other Bell states over two modes, which can be written as

$$|\psi\rangle = a|\mathrm{LP}_{01}\rangle|\mathrm{LP}_{1i}\rangle + b|\mathrm{LP}_{1i}\rangle|\mathrm{LP}_{01}\rangle (i \geq 1), \qquad (4)$$

where a and b are complex constants. We note that these LP_{1i} modes are eigenmodes of a fiber with noncircular geometry. Therefore an elliptic-core fiber without stress-applying materials is also suitable for our scheme. Since mode conversion relies on mechanical perturbation of the fiber core, the conversion efficiency does not strongly depend on the cladding structure. While higher-order modes can be guided by increasing the core size or the NA, a fiber with a larger core and a smaller NA generally has the advantages of stronger AO interaction and smaller modal dispersion.

Finally, we discuss the application of our method to long-distance transmission of entanglement. In the current experimental configuration, owing to the spectral entanglement of photon pairs, entanglement is preserved after the photons propagate through two equal-length fibers if the group delay between the LP_{01} and LP_{11} modes is smaller than the coherence time (nominally >160 ns) of the SPDC pump laser. This leads to a fiber length of up to tens of km. However, for general cases incorporating a different type of photon source or a different entangled state, the group delay needs to be smaller than the coherence time of photons. As the group velocity difference between spatial modes is a fraction of the difference between the core and cladding materials, the transmission distance through a standard fiber (NA $\sim$0.1) is limited to tens of cm per photonic spectral bandwidth of 1 nm. Two methods for relaxing this restriction are (1) choosing spatial modes propagating with the same group velocity, for example, the LP_{01} and LP_{11} modes in a fiber with normalized frequency $V \sim 3$, and (2) using a 100% mode converter in the middle of the transmission line to compensate for the group delay. When N spatial modes are used, a series of mode converters ($\mathrm{LP}_{01} \leftrightarrow \mathrm{LP}_{11}, \mathrm{LP}_{01} \leftrightarrow \mathrm{LP}_{12}, \ldots$) is placed for cyclic permutation at each of $(N-1)$ uniformly distributed points. A compact mode converter can be made from a long-period fiber grating [24].

In summary, we have demonstrated the transmission and measurement of the spatial entanglement of photons in two-mode optical fibers. Photonic spatial quantum states have been successfully measured by tunable all-fiber spatial filters based on acousto-optic interaction along the fibers. Observation of sinusoidal correlation fringes and measurements of concurrence have experimentally verified two-photon entanglement. The current scheme is extendable to higher-dimensional entanglement and hyperentanglement. We believe the present work provides a useful approach to quantum communications.

This work has been supported by the KRISS project "Convergent Science and Technology for Measurements at the Nanoscale."

*hspark@kriss.re.kr

[1] K. Mattle, H. Weinfurter, P. G. Kwiat, and A. Zeilinger, Phys. Rev. Lett. **76**, 4656 (1996).

[2] T. Jennewein, C. Simon, G. Weihs, H. Weinfurter, and A. Zeilinger, Phys. Rev. Lett. **84**, 4729 (2000).

[3] D. Bouwmeester, J.-W. Pan, M. Daniell, H. Weinfurter, and A. Zeilinger, Phys. Rev. Lett. **82**, 1345 (1999).
[4] A. Poppe, A. Fedrizzi, R. Ursin, H. Böhm, T. Lürunser, O. Maurhardt, M. Peev, M. Suda, C. Kurtsiefer, H. Weinfurter, T. Jennewein, and A. Zeilinger, Opt. Express **12**, 3865 (2004).
[5] T. Schmitt-Manderbach, H. Weier, M. Fürst, R. Ursin, F. Tiefenbacher, T. Scheidl, J. Perdigues, Z. Sodnik, C. Kurtsiefer, J. G. Rarity, A. Zeilinger, and H. Weinfurter, Phys. Rev. Lett. **98**, 010504 (2007).
[6] J. G. Rarity and P. R. Tapster, Phys. Rev. Lett. **64**, 2495 (1990).
[7] I. Marcikic, H. de Riedmatten, W. Tittel, V. Scarani, H. Zbinden, and N. Gisin, Phys. Rev. A **66**, 062308 (2002); I. Marcikic, H. de Riedmatten, W. Tittel, H. Zbinden, M. Legré, and N. Gisin, Phys. Rev. Lett. **93**, 180502 (2004).
[8] S. Ramelow, L. Ratschbacher, A. Fedrizzi, N. K. Langford, and A. Zeilinger, Phys. Rev. Lett. **103**, 253601 (2009).
[9] A. Mair, A. Vaziri, G. Weihs, and A. Zeilinger, Nature (London) **412**, 313 (2001).
[10] G. Gibson, J. Courtial, M. Padgett, M. Vasnetsov, V. Pas'ko, S. Barnett, and S. Franke-Arnold, Opt. Express **12**, 5448 (2004).
[11] A. Vaziri, G. Weihs, and A. Zeilinger, Phys. Rev. Lett. **89**, 240401 (2002).
[12] S. S. R. Oemrawsingh, X. Ma, D. Voigt, A. Aiello, E. R. Eliel, G. W. 't Hooft, and J. P. Woerdman, Phys. Rev. Lett. **95**, 240501 (2005).
[13] A. C. Dada, J. Leach, G. S. Buller, M. J. Padgett, and E. Andersson, Nature Phys. **7**, 677 (2011).
[14] J. T. Barreiro, T.-C. Wei, and P. G. Kwiat, Nature Phys. **4**, 282 (2008).
[15] L. Olislager, J. Cussey, A. T. Nguyen, P. Emplit, S. Massar, J.-M. Merolla, and K. P. Huy, Phys. Rev. A **82**, 013804 (2010).
[16] W. Löffler, T. G. Euser, E. R. Eliel, M. Scharrer, P. S. J. Russell, and J. P. Woerdman, Phys. Rev. Lett. **106**, 240505 (2011).
[17] S. H. Yun, I. K. Hwang, and B. Y. Kim, Opt. Lett. **21**, 27 (1996).
[18] B. Y. Kim, J. N. Blake, H. E. Engan, and H. J. Shaw, Opt. Lett. **11**, 389 (1986).
[19] J. P. Torres, A. Alexandrescu, and L. Torner, Phys. Rev. A **68**, 050301(R) (2003).
[20] H. E. Engan, B. Y. Kim, J. N. Blake, and H. J. Shaw, J. Lightwave Technol. **6**, 428 (1988).
[21] H. S. Park, K. Y. Song, S. H. Yun, and B. Y. Kim, J. Lightwave Technol. **20**, 1864 (2002).
[22] D. F. V. James, P. G. Kwiat, W. J. Munro, and A. G. White, Phys. Rev. A **64**, 052312 (2001).
[23] H. S. Kim, S. H. Yun, I. K. Hwang, and B. Y. Kim, Opt. Lett. **22**, 1476 (1997).
[24] A. M. Vengsarkar, P. J. Lemaire, J. B. Judkins, V. Bhatia, T. Erdogan, and J. E. Sipe, J. Lightwave Technol. **14**, 58 (1996).